

Reflection spectra from an accretion disc illuminated by a neutron star X-ray burst

D. R. Ballantyne[★]

Canadian Institute for Theoretical Astrophysics, 60 St. George Street, Toronto, Ontario, M5S 3H8, Canada

Accepted 2004 February 23. Received 2004 February 10; in original form 2004 January 15

ABSTRACT

Recent time-resolved X-ray spectra of a neutron star undergoing a superburst revealed an Fe $K\alpha$ line and edge consistent with reprocessing from the surrounding accretion disc. Here, we present models of X-ray reflection from a constant-density slab illuminated by a blackbody, the spectrum emitted by a neutron star burst. The calculations predict a prominent Fe $K\alpha$ line and a rich soft X-ray line spectrum which is superimposed on a strong free–free continuum. The lines slowly vanish as the ionization parameter of the slab is increased, but the free–free continuum remains dominant at energies less than 1 keV. The reflection spectrum has a quasi-blackbody shape only at energies greater than 3 keV. If the incident blackbody is added to the reflection spectrum, the Fe $K\alpha$ equivalent width varies between 100 and 300 eV depending on the ionization parameter and the temperature, kT , of the blackbody. The equivalent width is correlated with kT , and therefore we predict a strong Fe $K\alpha$ line when an X-ray burst is at its brightest (if iron is not too ionized or the reflection amplitude too small). Extending the study of reflection features in the spectra of superbursts to lower energies would provide further constraints on the accretion flow. If the Fe $K\alpha$ line or other features are relativistically broadened, then they can determine the system inclination angle (which leads to the neutron star mass), and, if the mass is known, a lower limit to the mass-to-radius ratio of the star.

Key words: accretion, accretion discs – line: profiles – radiative transfer – X-rays: binaries – X-rays: bursts.

1 INTRODUCTION

The reprocessing of external X-rays by accreting material has been observed from active galactic nuclei (AGN) and Galactic black hole candidates (GBHCs) for over a decade (e.g. Pounds et al. 1990; Nandra & Pounds 1994; Gierliński et al. 1999; Ballantyne, Vaughan & Fabian 2003; Miller et al. 2004). In these objects, the origin and location of the illuminating X-ray power-law is largely unknown, although it is widely believed to be either within a magnetic accretion disc corona (e.g. Galeev, Rosner & Vaiana 1979; Haardt & Maraschi 1993; Haardt, Maraschi & Ghisellini 1994; Di Matteo 1998) or a centrally located geometrically thick flow (e.g. Shapiro, Lightman & Eardley 1976; Zdziarski, Lubiński & Smith 1999; Zdziarski et al. 2003). Nevertheless, many models of X-ray reflection from black hole accretion discs have been computed (George & Fabian 1991; Matt, Perola & Piro 1991; Ross & Fabian 1993; Życki et al. 1994; Ross, Fabian & Young 1999; Nayakshin, Kazanas & Kallman 2000; Nayakshin & Kallman 2001; Ballantyne, Ross & Fabian 2001b; Różańska et al. 2002; Ballantyne, Turner & Blaes 2004), and, in some cases, successfully applied to data (Ballantyne, Iwasawa &

Fabian 2001a; Orr et al. 2001; De Rosa et al. 2002; Barrio, Done & Nayakshin 2003; Longinotti et al. 2003; Miller et al. 2004).

Recently, Strohmayer & Brown (2002) discovered an Fe $K\alpha$ line and edge in the X-ray spectra of the low-mass X-ray binary (LMXB) 4U 1820–30 as it was undergoing a superburst – a powerful thermonuclear explosion on the surface of the neutron star that can last many hours (Cornelisse et al. 2000; Strohmayer & Bildsten 2003; Kuulkers 2003). Based on the strength of the Fe $K\alpha$ line, these authors suggested that the features were caused by reflection of the burst blackbody spectrum from the surrounding accretion disc (e.g. Day & Done 1991). This hypothesis was supported by spectral fitting with detailed reflection models (Ballantyne & Strohmayer 2004). The unique aspect of reflection during a burst from a LMXB is that there is no uncertainty in the location of the X-ray source, as it is located on the surface of the neutron star and outshines the persistent X-ray emission from the disc. This fact allows for far less ambiguity when analysing changes to the reflection features, as they are more likely to trace the evolution in the accretion flow (Ballantyne & Strohmayer 2004).

X-ray emission lines have also been observed in the persistent emission from LMXBs (e.g. Smale et al. 1993; Angelini et al. 1995; Schulz 1999; Asai et al. 2000), and these are also thought to be caused by reprocessing by matter in the accretion flow (Shakura

[★]E-mail: ballantyne@cita.utoronto.ca

& Sunyaev 1973; Meyer & Meyer-Hofmeister 1982). The spectral shape of the persistent emission is consistent with bremsstrahlung with a temperature of 5–10 keV (Liu, van Paradijs & van den Heuvel 2001), most likely arising from the boundary layer between the disc and the neutron star. Detailed models of the photoionized layer on the disc have been performed and predict a wealth of emission lines in the soft X-ray band (e.g. Ko & Kallman 1994; Jimenez-Garate, Raymond & Liedahl 2002) that can be compared against observations made with the grating spectrometers on board *Chandra* and *XMM-Newton* (e.g. Cottam et al. 2001; Schulz et al. 2001; Kallman et al. 2003). In contrast, a X-ray burst emits a blackbody spectrum (Hoffman, Lewin & Doty 1977; Swank et al. 1977), and can reach the Eddington luminosity ($L_{\text{Edd}} \sim 10^{38} \text{ erg s}^{-1}$), over 10 times greater than the persistent luminosity of many LMXBs (Strohmayer & Bildsten 2003). Thus, disc reflection will be dominated by the blackbody component during the burst.

This paper presents reflection spectra from a uniform accretion disc illuminated by a blackbody, as in a LMXB during a Type IX-ray (super)burst. These spectra were used to fit the superburst data of 4U 1820–30 (Ballantyne & Strohmayer 2004), but, as shown below, they contain much more information than what was actually needed for those *Rossi X-ray Timing Explorer (RXTE)* data. Observations of reflection features from Type I bursts or superbursts with sensitive, large-bandwidth instruments such as the X-ray Telescope (XRT) on *Swift* could provide a wealth of new information on the structure and behaviour of accretion discs.

In the next section, we outline the reflection calculations, and we present the resulting spectra in Section 3. We conclude by discussing the results in Section 4.

2 CALCULATIONS

The reflection spectra were computed using the code of Ross & Fabian (1993). Details of the computational techniques can be found in that paper and in references therein (see also Ross et al. 1999 and Ballantyne et al. 2001b), and so only a brief overview will be presented here.

A one-dimensional slab of material with a constant hydrogen number density n_{H} is illuminated by a blackbody spectrum with temperature kT and flux (defined between 1 eV and 100 keV) F_{X} . Thus, we define the ionization parameter

$$\xi = \frac{4\pi F_{\text{X}}}{n_{\text{H}}} \quad (1)$$

The input radiation is transferred into the layer using the two-stream approximation (Rybicki & Lightman 1979) while the outgoing radiation is treated using the modified Fokker–Planck/diffusion method of Ross, Weaver & McCray (1978). Therefore, the output spectrum is averaged over all viewing angles. The ionization and thermal structure of the illuminated gas is iterated until each zone reaches ionization and thermal balance, and at this point the final reflection spectrum is computed. The illuminated slab always has a large enough Thomson depth ($\tau_{\text{T}} = 6\text{--}20$, depending on ξ) so that the highest-energy photons will interact many times with the gas. The cosmic abundances of Morrison & McCammon (1983) were assumed, but hydrogen and helium are taken to be completely ionized at all times (i.e. $n_{\text{e}} = 1.2n_{\text{H}}$). The following ionization stages of the most important astrophysical metals are treated in the calculation: C V–VII, N VI–VIII, O V–IX, Mg IX–XIII, Si XI–XV and Fe XVI–XXVII.

Models were calculated for $1 \leq kT \leq 3.15$ keV, as this spans the range most often observed during X-ray bursts (Kuulkers 2003),

and for $1 \leq \log \xi \leq 3.75$. To change ξ , n_{H} was fixed at 10^{15} cm^{-3} , and F_{X} was varied.

3 RESULTS

We begin by considering the evolution of the reflection spectra as a function of ξ (cf. fig. 2 in Ross et al. 1999). Fig. 1 shows a series of spectra for four different values of kT . Each panel shows reflection spectra with $\log \xi = 1, 1.5, 2, 2.5, 3$ and 3.5 (from bottom to top), thereby spanning the range from very weakly ionized reflectors to highly ionized ones. For the $\log \xi = 2$ model, we have also plotted the incident blackbody spectrum.

Unlike the power-law continua of AGN and GBHCs, in which the radiant energy per frequency decade reaches a maximum at energies > 10 keV (for photon indices $\Gamma < 2$) where atomic absorption is minimal, the blackbody spectra peak at energies where the photoelectric absorption by metals is very important. As a result, only a small fraction of the photons incident on the slab are scattered back without first being absorbed by an ion. The reflection spectra therefore only mimic a blackbody at energies $E \gtrsim 3$ keV, with the agreement increasing as $\log \xi$ grows and as the metals are ionized. The energy absorbed by the metals in the gas is thermalized and re-emerges as a strong soft free–free continuum with a variety of recombination lines superimposed. As this thermal emission includes the power absorbed at higher energies, it outshines the incident blackbody at $E \lesssim 1$ keV for all values of ξ considered. The rich emission-line spectrum is reminiscent of those predicted from models of reprocessing of the persistent emission (Jimenez-Garate et al. 2002). However, in the most luminous stage of an X-ray burst, the disc may be severely ionized (Ballantyne & Strohmayer 2004), and will leave a Compton-broadened O VIII Ly α line as the only emission feature in the soft X-ray region of the spectrum.

It is instructive to look at the most important heating and cooling processes within the illuminated layer. A plot of the heating and cooling rates as a function of Thomson depth into the slab for the $\log \xi = 3, kT = 2.5$ keV model is shown in the lower panel of Fig. 2. In this figure, the heating and cooling processes are shown by red and blue lines, respectively, while the different line styles separate the physical process (for example, Compton heating is denoted by the red dotted line, but Compton cooling is shown with the blue dotted line). The upper panel of Fig. 2 shows the final iron ionization structure in the slab. Hydrogenic iron dominates between the surface and the first Thomson depth, but recombines to He-like iron before reaching $\tau_{\text{T}} = 2$. The iron recombines rapidly just beyond this point and reaches the lowest ionization stage treated (Fe XVI) at $\tau_{\text{T}} \approx 5$. Turning to the heating and cooling rates, we see that free–free emission is the dominant cooling mechanism over the entire depth of the slab. At the surface, where the gas temperature reaches $\sim 5 \times 10^6$ K (the black line in the lower panel of Fig. 2), the bremsstrahlung cooling is balanced by Compton and photoelectric heating. However, the Compton heating rate falls rapidly with τ_{T} because there are very few high-energy photons in the incident blackbody spectra. In contrast, the photoelectric heating rate increases with τ_{T} until it reaches a maximum at $\tau_{\text{T}} \sim 3$, where iron is rapidly recombining (upper panel of Fig. 2) and the photoionization rates jumps. The line cooling rate also increases rapidly here but cannot overcome the free–free cooling. After the iron has almost fully recombined at $\tau_{\text{T}} \sim 5$, the photoelectric heating rate falls (very few ionizing photons can penetrate to such depths) and the dominant heating process becomes free–free absorption. The line-cooling rate jumps one more time at $\tau_{\text{T}} \sim 9$, where oxygen is recombining (note the

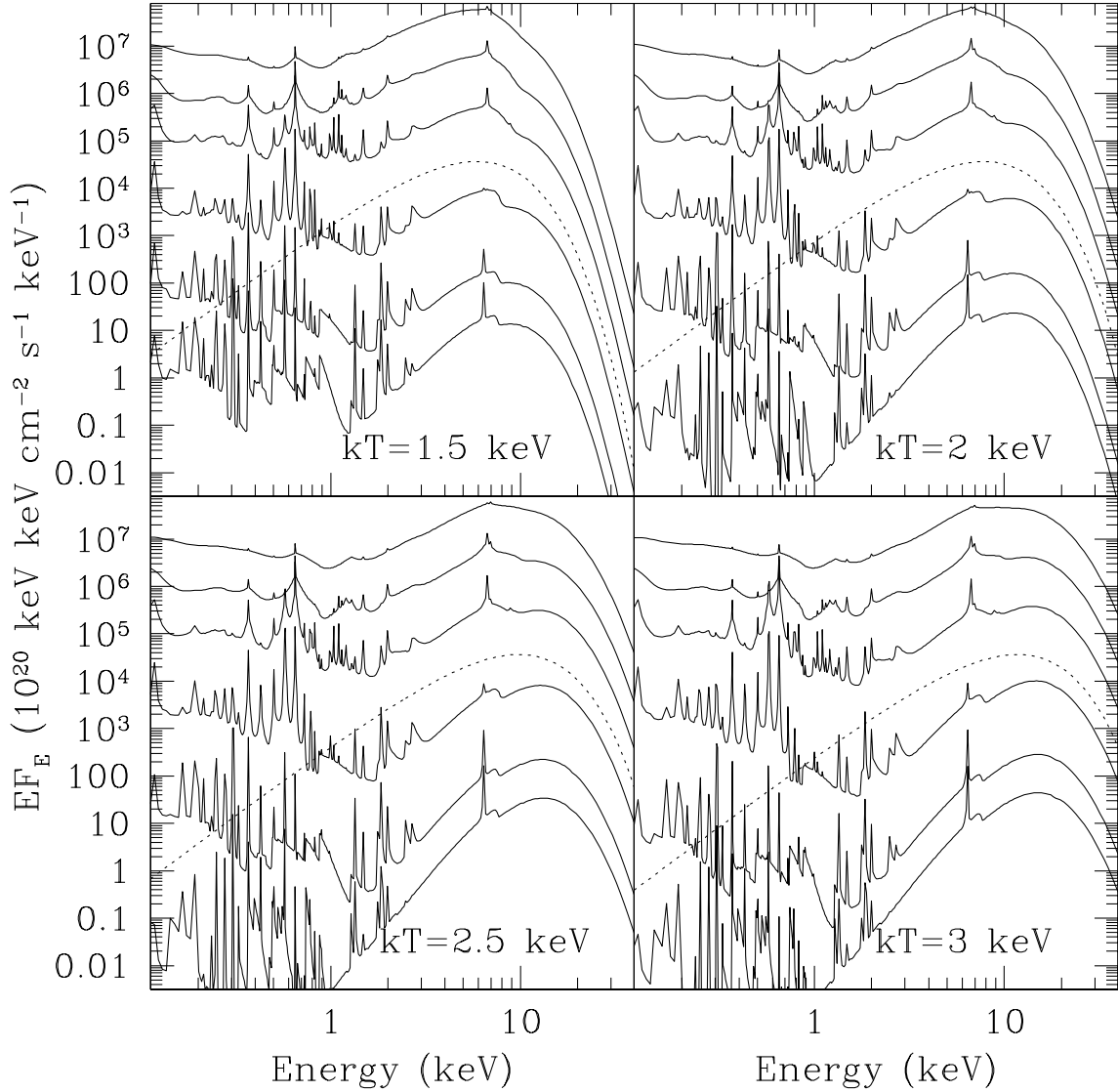


Figure 1. Examples of reflection spectra from an accretion disc illuminated by a blackbody continuum. The four panels show results for different values of kT . Within each panel, six reflection spectra are shown with solid lines. They denote models with (moving from bottom to top) $\log \xi = 1, 1.5, 2, 2.5, 3$ and 3.5 . All of the spectra, except for the $\log \xi = 2$ model, have been vertically offset from one another for clarity. The dotted line in each panel shows the illuminating blackbody for the $\log \xi = 2$ model.

corresponding fall in the gas temperature). The dominance of free-free cooling and photoelectric heating in the thermal structure of the illuminated slab emphasizes the dominance of the absorption-thermalization process in these models. The observational outcome is the rich X-ray line spectrum seen below 1 keV in Fig. 1.

Similar to the reflection spectra predicted for the environment of accreting black holes, the Fe $K\alpha$ line is the most important spectral feature above ~ 3 keV in the blackbody models, and is an important indicator of the ionization parameter of the reflecting medium. Fig. 1 shows that, in each panel, the Fe $K\alpha$ line evolves from a strong 6.4-keV line to a weak, Auger-destroyed line, and then to a broad 6.7-keV feature before disappearing entirely due to the complete ionization of iron. This is the same sequence as that presented by Ross et al. (1999) for illumination by a power law.

The equivalent width (EW) of the Fe $K\alpha$ line as a function of $\log \xi$ is shown in Fig. 3. The top panel shows the EWs measured from the reflection spectra themselves, while the lower panel includes

the diluting effect of adding in the incident blackbody that will also be observed along with the reflection spectrum. The measurements were made for the four values of kT shown in Fig. 1, and for 75 values of $\log \xi$ between 1 and 3.75. There are two peaks in the EW evolution: one when $\log \xi \approx 1$ and Fe $K\alpha$ is at 6.4 keV, and the other when $\log \xi \approx 2.7$ and the line is at 6.7 keV. The EW of the cold line is much stronger than the ionized one in the case of pure reflection, but is switched when the incident blackbody is included. This is because, at larger values of ξ , there is less metal absorption in the illuminated slab and the reflection spectrum is not as diluted by the blackbody as in the low- ξ models.

The Fe $K\alpha$ EW is a strong linear function of the temperature of the blackbody; for example, when $\log \xi = 1$ and the incident blackbody is included, the EW increases from ~ 70 eV (at $kT = 1.5$ keV) to 180 eV (at $kT = 3$ keV). This is a result of the increase in photons above the Fe K edge (at 7.1–9 keV) as kT is increased. This has important implications for the study of X-ray bursts, because the

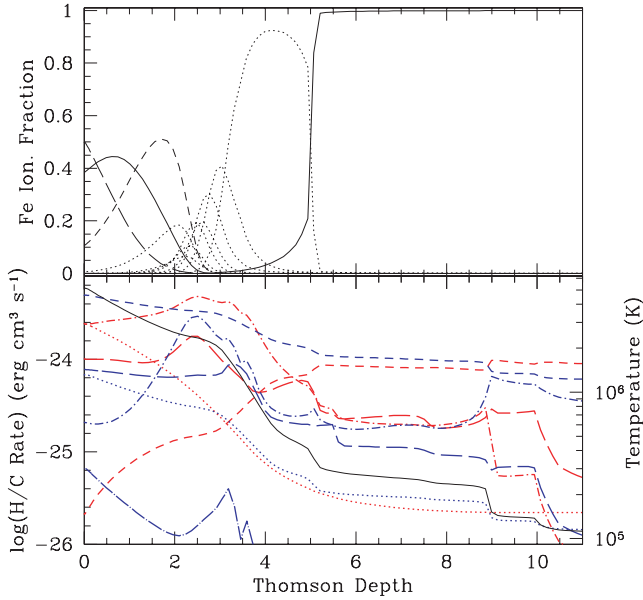


Figure 2. Details from the $\log \xi = 3$, $kT = 2.5$ keV reflection calculation as a function of Thomson depth into a slab with $n_H = 10^{15} \text{ cm}^{-3}$. The upper panel plots the iron ionization structure. Moving from the surface down into the slab, the iron ions encountered are Fe XXVII (long-dashed line), hydrogenic Fe XXVI (solid line), Fe XXV (short-dashed line), Fe XVII–XXIV (dotted lines) and Fe XVI (solid line; the most neutral iron ion treated). The lower panel plots the heating (H, red curves) and cooling (C, blue curves) rates and the gas temperature (right-hand axis; black solid line). The line types distinguish the various physical processes: Compton heating/cooling (dotted lines), free–free heating/cooling (short-dashed lines), recombination heating/cooling (long-dashed lines), photoelectric heating/line cooling (dot–short-dashed lines) and three-body interactions (dot–long-dashed lines).

blackbody emission is at its hottest when the burst is brightest. Therefore, unless iron is fully ionized by the burst (i.e. $\log \xi > 3.7$), the Fe $K\alpha$ line should be most prominent at the point where the burst is most easily observable. However, a superburst may cause changes in the accretion geometry close to the neutron star which would reduce the reflection amplitude and the EW of the Fe $K\alpha$ line (Ballantyne & Strohmayer 2004).

4 DISCUSSION

Searches for spectral features during X-ray bursts from neutron stars have been ongoing for many years. Because the explosion is occurring on the surface of the star, the spectral features would be expected to be redshifted and would therefore be a measure of the mass-to-radius ratio of the star [via $1 + z = (1 - GM/c^2 R)^{-1/2}$], a number needed to constrain the many possible equations of state of nuclear matter. During the 1980s, there were a few reports of X-ray absorption lines at 4.1 keV during Type I X-ray bursts (Waki et al. 1984; Nakamura, Inoue & Tanaka 1988; Magnier et al. 1989), which were interpreted as redshifted Ly α absorption from He-like iron. However, the equivalent width of these absorption lines were on the order of hundreds of eV, which theoretical models of spectral formation in burst atmospheres could not reproduce (Foster, Ross & Fabian 1987; Day, Fabian & Ross 1992). Observations by more sensitive instruments on *RXTE* and *BeppoSAX* have been unable to discover any other examples of a 4.1-keV absorption line. Recently, the Reflection Grating Spectrometer (RGS) on *XMM–Newton* has uncovered evidence for redshifted absorption lines during the X-ray

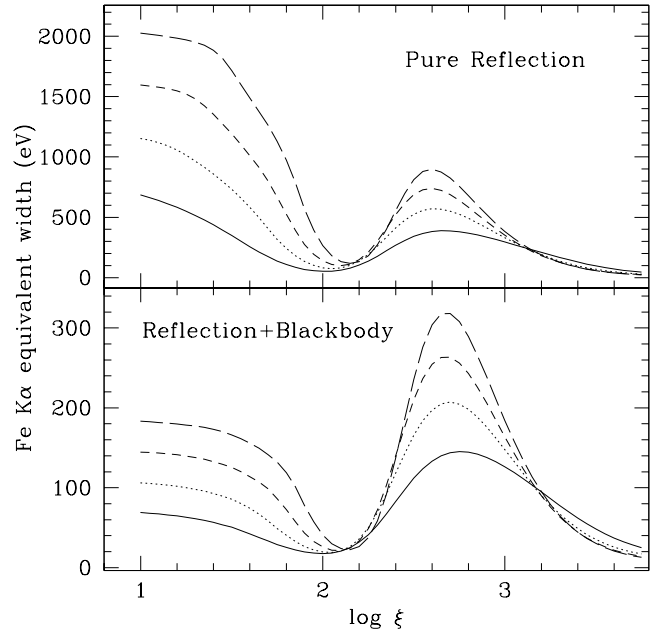


Figure 3. The Fe $K\alpha$ equivalent width (EW) as a function of $\log \xi$ for the four values of kT shown in Figure 1. The upper panel plots the EW measured from the pure reflection spectrum (i.e. there is no contribution from the blackbody). The lower panel plots the EW measured from the sum of the reflected and incident spectra. In both panels, the different line types separate the values of kT : 1.5 keV (solid line), 2 keV (dotted line), 2.5 keV (short-dashed line), and 3 keV (long-dashed line).

bursts of EXO 0748-676 (Cottam et al. 2002), although data from 28 bursts were needed in order to obtain the minimum signal-to-noise necessary to find the lines.

As first suggested by Day & Done (1991), X-rays from an explosion on a neutron star can be reprocessed by the surrounding accretion disc, leading to features such as an Fe $K\alpha$ line and edge. The analysis of these features can lead to many new insights about the structure and evolution of the accretion disc (Ballantyne & Strohmayer 2004), as well as basic information about the neutron star itself. For example, if the emission lines are relativistically broadened, then modelling can reveal the inclination angle of the system to the line of sight (Fabian et al. 1989), a parameter often needed to obtain masses of the neutron star and its binary companion. Modelling of relativistic lines also produce a radius where the reflection originates (assuming some emissivity profile). This radius is measured in gravitational units (GM/c^2), so if the mass of the neutron star is known, the radius can be converted to physical units, allowing a determination of a mass-to-radius ratio. Because the reflection may occur very close to the surface of the neutron star ($10\text{--}20 GM/c^2$ in 4U 1820–30; Ballantyne & Strohmayer 2004), the measurement may provide a useful lower limit to the mass-to-radius ratio for the neutron star.

RXTE has so far been the most successful telescope to obtain time-resolved spectroscopy of X-ray bursts, especially of the more energetic superbursts (e.g. Strohmayer & Brown 2002). The telescope produces data for energies greater than 3 keV, which allows a good determination of the blackbody spectrum and, if detected, the Fe $K\alpha$ line. Yet, the reflection models predict a wealth of information at energies less than 3 keV (Fig. 1) that can provide further constraints on the abundances, ionization state and dynamics of the accretion disc. These features will also strongly depend on the

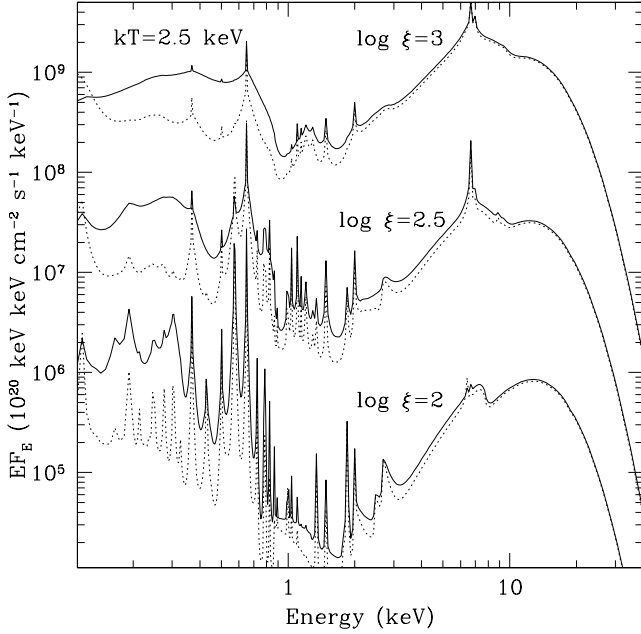


Figure 4. The solid lines show three reflection spectra computed with a density of $n_{\text{H}} = 10^{18} \text{ cm}^{-3}$, while the dotted lines denote models with identical ξ but with $n_{\text{H}} = 10^{15} \text{ cm}^{-3}$. A $kT = 2.5 \text{ keV}$ blackbody was the illuminating continuum for all cases. The increase in density results in only minor differences in the spectra at energies $\gtrsim 3 \text{ keV}$, but there are significant changes at lower energies.

density of the disc because of the importance of collisional effects and free–free emission/absorption. The spectra shown in Fig. 1 were calculated assuming a density of $n_{\text{H}} = 10^{15} \text{ cm}^{-3}$, appropriate for the outer regions of the disc. The density at a distance of a few gravitational radii from the neutron star is expected to be $> 10^{21} \text{ cm}^{-3}$, even for a radiation-pressure dominated disc (Shakura & Sunyaev 1973), which is beyond the range of validity for the reflection code. To illustrate the effects of higher density on the soft X-ray spectrum, Fig. 4 compares three reflection spectra computed with $n_{\text{H}} = 10^{15} \text{ cm}^{-3}$ with ones computed at 10^{18} cm^{-3} , where the code remains valid. The figure shows very little difference in the spectra in the *RXTE* band including the Fe $K\alpha$ line. This implies that the Fe $K\alpha$ EWs computed from the $n_{\text{H}} = 10^{15} \text{ cm}^{-3}$ models (Fig. 3) should still be useful guidelines for future observations. On the other hand, the 1000-fold increase in density significantly alters the soft X-ray features predicted by the reflection spectra. The differences mainly lie at energies $< 0.5 \text{ keV}$, where the continuum level is raised due to the increase in free–free emission and absorption. As a result, the EWs of many of the emission lines have been substantially decreased. The expectation is that increasing the density further will continue to raise the continuum level at soft energies, as more line emission is absorbed by the continuum, and that it will decrease the EW of the remaining emission lines. Clearly, the soft X-ray emission features are a strong diagnostic for the accretion disc density. It would be therefore be very interesting to obtain rapid, time-resolved broad-band spectra of X-ray bursts to exploit the information in those spectral features. In the near future, only the XRT on board the *Swift* satellite will have these features, plus the necessary rapid response capability. Unfortunately, soft X-ray spectroscopy of burst sources will be challenging. LMXBs are old systems and many of them lie toward to the Galactic centre, thus suffering from significant absorption due to neutral hydrogen along the line of sight.

However, there are a number of LMXBs which reside in globular clusters that may provide lower extinction columns and allow sensitive soft X-ray observations. Rapid follow-up of X-ray bursts from LMXB globular clusters therefore provide the best chance of utilizing the full information obtained in the reflection spectra.

ACKNOWLEDGMENTS

The author thanks R. Ross and A. Fabian for advice on the reflection models, and acknowledges financial support from the Natural Sciences and Engineering Research Council of Canada.

REFERENCES

- Angelini L., White N. E., Nagase F., Kallman T. R., Yoshida A., Takeshima T., Becker C., Paerels F., 1995, *ApJ*, 449, L41
- Asai K., Dotani T., Nagase F., Mitsuda K., 2000, *ApJS*, 131, 571
- Ballantyne D. R., Strohmayer T. E., 2004, *ApJ*, 602, L105
- Ballantyne D. R., Iwasawa K., Fabian, A. C., 2001a, *MNRAS*, 323, 506
- Ballantyne D. R., Ross R. R., Fabian A. C., 2001b, *MNRAS*, 327, 10
- Ballantyne D. R., Vaughan S., Fabian A. C., 2003, *MNRAS*, 342, 239
- Ballantyne D. R., Turner N. J., Blaes O. M., 2004, *ApJ*, 603, 436
- Barrio F. E., Done C., Nayakshin S., 2003, *MNRAS*, 342, 557
- Cornelisse R., Heise J., Kuulkers E., Verbunt F., in 't Zand J. J. M., 2000, *A&A*, 357, L21
- Cottam J., Sako M., Kahn S. M., Paerels F., Liedahl D. A., 2001, *ApJ*, 557, L101
- Cottam J., Paerels F., Mendez M., 2002, *Nat*, 420, 51
- Day C. S. R., Done C., 1991, *MNRAS*, 253, p. 35
- Day C. S. R., Fabian A. C., Ross R. R., 1992, *MNRAS*, 257, 471
- De Rosa A., Piro L., Fiore F., Grandi P., Maraschi L., Matt G., Nicastro F., Petrucci P. O., 2002, *A&A*, 387, 838
- Di Matteo T., 1998, *MNRAS*, 299, L15
- Fabian A. C., Rees M. J., Stella L., White N. E., 1989, *MNRAS*, 238, 729
- Foster A. J., Ross R. R., Fabian A. C., 1987, *MNRAS*, 228, 259
- Galeev A. A., Rosner R., Vaiana G. S., 1979, *ApJ*, 229, 318
- George I. M., Fabian A. C., 1991, *MNRAS*, 249, 352
- Gierliński M., Zdziarski A. A., Poutanen J., Coppi P. S., Ebisawa K., Johnson W. N., 1999, *MNRAS*, 309, 496
- Haardt F., Maraschi L., 1993, *ApJ*, 413, 507
- Haardt F., Maraschi L., Ghisellini G., 1994, *ApJ*, 432, L95
- Hoffman J. A., Lewin W. H. G., Doty J., 1977, *ApJ*, 217, L23
- Jimenez-Garate M. A., Raymond J. C., Liedahl D. A., 2002, *ApJ*, 581, 1297
- Kallman T. R., Angelini L., Boroson B., Cottam J., 2003, *ApJ*, 583, 861
- Ko Y.-K., Kallman T. R., 1994, *ApJ*, 431, 273
- Kuulkers E., 2003, in van den Heuvel E. P. J., in 't Zand J. J. M., Wijers R. A. M. J., eds, *The Restless High-Energy Universe*. Elsevier, Amsterdam (astro-ph/0310402)
- Liu Q. Z., van Paradijs J., van den Heuvel E. P. J., 2001, *A&A*, 368, 1021
- Longinotti A. L., Cappi M., Nandra K., Dadina M., Pellegrini S., 2003, *A&A*, 410, 471
- Magnier E., Lewin W. H. G., van Paradijs J., Tan J., Penninx W., Damen E., 1989, *MNRAS*, 237, 729
- Matt G., Perola G. C., Piro L., 1991, *A&A*, 247, 25
- Meyer F., Meyer-Hofmeister E., 1982, *A&A*, 106, 34
- Miller J. M. et al., 2004, *ApJ*, 601, 450
- Morrison R., McCammon D., 1983, *ApJ*, 270, 119
- Nakamura N., Inoue H., Tanaka Y., 1988, *PASJ*, 40, 209
- Nandra K., Pounds K. A., 1994, *MNRAS*, 268, 405
- Nayakshin S., Kallman T. R., 2001, *ApJ*, 546, 406
- Nayakshin S., Kazanas D., Kallman T. R., 2000, *ApJ*, 537, 833
- Orr A., Barr P., Guainazzi M., Parmar A. N., Young, A. J., 2001, *A&A*, 376, 413
- Pounds K. A., Nandra K., Stewart G. C., George I. M., Fabian A. C., 1990, *Nat*, 344, 132

- Ross R. R., Fabian A. C., 1993, MNRAS, 261, 74
Ross R. R., Weaver R., McCray R., 1978, ApJ, 219, 292
Ross R. R., Fabian A. C., Young A. J., 1999, MNRAS, 306, 461
Róžańska A., Dumont A.-M., Czerny B., Collin S., 2002, MNRAS, 332, 799
Rybicki G. B., Lightman A. P., 1979, Radiative Processes in Astrophysics. Wiley, New York
Schulz N. S., 1999, ApJ, 511, 304
Schulz N. S., Chakrabarty D., Marshall H. L., Canizares C. R., Lee J. C., Houck J., 2001, ApJ, 563, 941
Shakura N. I., Sunyaev R. A., 1973, A&A, 24, 337
Shapiro S. L., Lightman A. P., Eardley D. M., 1976, ApJ, 204, 187
Smale A. P. et al., 1993, ApJ, 410, 796
Strohmayer T. E., Brown E. F., 2002, ApJ, 566, 1045
Strohmayer T. E., Bildsten L., 2003, in Lewin W. H. G., van der Klis M., eds, Compact Stellar X-ray Sources. Cambridge Univ. Press, Cambridge, in press (astro-ph/0301544)
Swank J. H., Becker R. H., Boldt E. A., Holt S. S., Pravdo S. H., Serlemitsos P. J., 1977, ApJ, 212, L73
Waki I. et al., 1984, PASJ, 36, 819
Zdziarski A. A., Lubiński P., Smith D. A., 1999, MNRAS, 303, 11
Zdziarski A. A., Lubiński P., Gilfanov M., Revnivtsev M., 2003, MNRAS, 342, 355
Życki P. T., Krolik J. H., Zdziarski A. A., Kallman T. R., 1994, ApJ, 437, 597

This paper has been typeset from a \TeX/L\AA\TeX file prepared by the author.